A strategy for quantitative spectral imaging of tissue absorption and scattering using light emitting diodes and photodiodes

Justin Y. Lo,[1,*] Bing Yu,[1] Henry L. Fu,[1] Janelle E. Bender,[1] Gregory M. Palmer,[2] Thomas F. Kuech,[3] and Nirmala Ramanujam[1]

[1]*Department of Biomedical Engineering, Duke University, Durham, NC 27708, USA*
[2]*Department of Radiation Oncology, Duke University, Durham, NC 27708, USA*
[3]*Department of Chemical and Biological Engineering, University of Wisconsin, Madison, WI 53706, USA*
[*]*Corresponding author: justin.lo@duke.edu*

Abstract: A diffuse reflectance spectroscopy system was modified as a step towards miniaturization and spectral imaging of tissue absorption and scattering. The modified system uses a tunable source and an optical fiber for illumination and a photodiode in contact with tissue for detection. Compared to the previous system, it is smaller, less costly, and has comparable performance in extracting optical properties in tissue phantoms. Wavelength reduction simulations show the feasibility of replacing the source with LEDs to further decrease system size and cost. Simulated crosstalk analysis indicates that this evolving system can be multiplexed for spectral imaging in the future.

OCIS codes: 170.4580 (Optical diagnostics for medicine); 170.6510 (Spectroscopy, tissue diagnostics)

References and links

1. B.J. Moeller, R.A. Richardson, and M.W. Dewhirst, "Hypoxia and radiotherapy: opportunities for improved outcomes in cancer treatment," Cancer Metastasis Rev. **26**, 241-248 (2007).
2. E.J. Moon, D.M. Brizel, J.T. Chi, and M.W. Dewhirst, "The potential role of intrinsic hypoxia markers as prognostic variables in cancer," Antioxid. Redox Signal. **9**, 1237-1294 (2007).
3. A.A. Stratonnikov and V.B. Loschenov, "Evaluation of blood oxygen saturation in vivo from diffuse reflectance spectra," J. Biomed. Opt. **6**, 457-467 (2001).
4. I.J. Bigio, S.G. Bown, G. Briggs, C. Kelley, S. Lakhani, D. Pickard, P.M. Ripley, I.G. Rose, and C. Saunders, "Diagnosis of breast cancer using elastic-scattering spectroscopy: preliminary clinical results," J. Biomed. Opt. **5**, 221-228 (2000).
5. S.K. Chang, Y.N. Mirabal, E.N. Atkinson, D. Cox, A. Malpica, M. Follen, and R. Richards-Kortum, "Combined reflectance and fluorescence spectroscopy for in vivo detection of cervical pre-cancer," J. Biomed. Opt. **10**, 024031 (2005).
6. G. Zonios, L.T. Perelman, V. Backman, R. Manoharan, M. Fitzmaurice, J. Van Dam, and M.S. Feld, "Diffuse Reflectance Spectroscopy of Human Adenomatous Colon Polyps In Vivo," Appl. Opt. **38**, 6628-6637 (1999).
7. R. Reif, O. A'Amar, and I.J. Bigio, "Analytical model of light reflectance for extraction of the optical properties in small volumes of turbid media," Appl. Opt. **46**, 7317-7328 (2007).
8. R. Reif, M.S. Amorosino, K.W. Calabro, O. A'Amar, S.K. Singh, and I.J. Bigio, "Analysis of changes in reflectance measurements on biological tissues subjected to different probe pressures," J. Biomed. Opt. **13**, 010502 (2008).
9. W.C. Lin, S.A. Toms, M. Johnson, E.D. Jansen, and A. Mahadevan-Jansen, "In vivo brain tumor demarcation using optical spectroscopy," Photochem. Photobiol. **73**, 396-402 (2001).
10. A. Cerussi, D. Hsiang, N. Shah, R. Mehta, A. Durkin, J. Butler, and B.J. Tromberg, "Predicting response to breast cancer neoadjuvant chemotherapy using diffuse optical spectroscopy," Proc. Natl Acad. Sci. U.S.A. **104**, 4014-4019 (2007).
11. D.B. Jakubowski, A.E. Cerussi, F. Bevilacqua, N. Shah, D. Hsiang, J. Butler, and B.J. Tromberg, "Monitoring neoadjuvant chemotherapy in breast cancer using quantitative diffuse optical spectroscopy: a case study," J. Biomed. Opt. **9**, 230-238 (2004).

#103335 - $15.00 USD Received 28 Oct 2008; revised 15 Jan 2009; accepted 16 Jan 2009; published 22 Jan 2009

12. N. Shah, J. Gibbs, D. Wolverton, A. Cerussi, N. Hylton, and B.J. Tromberg, "Combined diffuse optical spectroscopy and contrast-enhanced magnetic resonance imaging for monitoring breast cancer neoadjuvant chemotherapy: a case study," J. Biomed. Opt. **10**, 051503 (2005).
13. I.J. Bigio and S.G. Bown, "Spectroscopic sensing of cancer and cancer therapy: current status of translational research," Cancer Biol. Ther. **3**, 259-267 (2004).
14. J. Lee, A.E. Cerussi, D. Saltzman, T. Waddington, B.J. Tromberg, and M. Brenner, "Hemoglobin measurement patterns during noninvasive diffuse optical spectroscopy monitoring of hypovolemic shock and fluid replacement," J. Biomed. Opt. **12**, 024001 (2007).
15. T.J. Pfefer, L.S. Matchette, C.L. Bennett, J.A. Gall, J.N. Wilke, A.J. Durkin, and M.N. Ediger, "Reflectance-based determination of optical properties in highly attenuating tissue," J. Biomed. Opt. **8**, 206-215 (2003).
16. G.M. Palmer and N. Ramanujam, "Monte Carlo-based inverse model for calculating tissue optical properties. Part I: Theory and validation on synthetic phantoms," Appl. Opt. **45**, 1062-1071 (2006).
17. G.M. Palmer, C. Zhu, T.M. Breslin, F. Xu, K.W. Gilchrist, and N. Ramanujam, "Monte Carlo-based inverse model for calculating tissue optical properties. Part II: Application to breast cancer diagnosis," Appl. Opt. **45**, 1072-1078 (2006).
18. C. Zhu, G.M. Palmer, T.M. Breslin, J. Harter, and N. Ramanujam, "Diagnosis of breast cancer using diffuse reflectance spectroscopy: Comparison of a Monte Carlo versus partial least squares analysis based feature extraction technique," Lasers Surg. Med. **38**, 714-724 (2006).
19. C. Zhu, G.M. Palmer, T.M. Breslin, F. Xu, and N. Ramanujam, "Use of a multiseparation fiber optic probe for the optical diagnosis of breast cancer," J. Biomed. Opt. **10**, 024032 (2005).
20. M.C. Skala, G.M. Palmer, K.M. Vrotsos, A. Gendron-Fitzpatrick, and N. Ramanujam, "Comparison of a physical model and principal component analysis for the diagnosis of epithelial neoplasias in vivo using diffuse reflectance spectroscopy," Opt. Express. **15**, 7863-7875 (2007).
21. V.T. Chang, P.S. Cartwright, S.M. Bean, G.M. Palmer, R. Bentley, and N. Ramanujam, "Quantitative physiology of the precancerous cervix *in vivo* via optical spectroscopy," Neoplasia. (to be published).
22. J.E. Bender, K. Vishwanath, L.K. Moore, J.Q. Brown, V. Chang, G.M. Palmer, and N. Ramanujam, "A robust Monte Carlo model for the extraction of biological absorption and scattering *in vivo*," IEEE Trans. Biomed. Eng. (to be published).
23. W.F. Cheong, "Appendix to chapter 8: Summary of optical properties," Optical-Thermal Response of Laser-Irradiated Tissue. 275-303 (1995).
24. S. Prahl, "Mie scattering program," Oregon Medical Laser Center. (2005).
25. J.B. Fishkin, O. Coquoz, E.R. Anderson, M. Brenner, and B.J. Tromberg "Frequency-domain photon migration measurements of normal and malignant tissue optical properties in a human subject," Appl. Opt. **36**, 10-20 (1997).

1. Introduction

The ability to quantify tissue physiological and morphological properties can have tremendous impact in many clinical situations, potentially improving the clinical management and care of patients [1, 2]. Because diffuse reflectance spectroscopy in the UV-visible spectral range is sensitive to the absorption and scattering properties of biological molecules, such as hemoglobin, cell nuclei, and mitochondria, several groups have investigated the technology as a tool for monitoring tissue oxygenation [3], pre-cancer and cancer detection [4-8], tumor margin assessment [9], assessing tumor response to therapy [10-12], and in other biomedical applications [13-15]. We have previously developed a fiber-optic based diffuse reflectance spectroscopy system consisting of a xenon lamp, monochromator and CCD camera (benchtop system) and a fast inverse Monte Carlo model of reflectance to quantify tissue absorption and scattering of turbid media such as tissues and applied it in a variety of pre-clinical and clinical applications to date [16-19].

Although our toolbox is capable of effectively quantifying tissue absorption and scattering [17-20], like other diffuse reflectance spectrometers, the system has drawbacks in cost, collection efficiency, and clinical relevance and utility, which is of utmost importance to physicians and patients. First, the current technology is a single-point sampling system in nature and is not ideal for applications where there is a need to cover large sampling areas, such as in tumor margin assessment or cervical or skin cancer detection. While single-point fiber-optic based detection is reasonable for a few and very small regions of interest [5, 21], it can be very cumbersome and expensive when expanded for use in quantitative spectral imaging. Furthermore, optical fibers generally collect only a small portion of the remitted

#103335 - $15.00 USD Received 28 Oct 2008; revised 15 Jan 2009; accepted 16 Jan 2009; published 22 Jan 2009

signal, thus requiring the costly high quantum efficiency, ultra-low noise CCDs, particularly in the UV-VIS region. Thus obviating the need for optical fibers in detection could potentially improve throughput.

In this article, we present the simple design and validation of a new probe to quantify absorption and scattering based on an inexpensive, robust silicon photodiode integrated with a single illumination fiber coupled to a xenon lamp and monochromator, which eliminates the need for costly detection equipment and optical fibers for collection. The probe was tested in liquid tissue phantoms, and optical properties were extracted with the inverse Monte Carlo model of reflectance developed by our group [16, 17]. The performance of the new probe was compared with that of the original benchtop system mentioned above. Wavelength reduction simulations were also performed to assess the feasibility of replacing the tunable light source with several miniature LEDs, further reducing the size and cost of the current system. In addition, a preliminary crosstalk analysis was done to show the potential for multiplexing the system into an imaging device, which could ultimately quantify tissue physiological and morphological properties over a large field of view.

2. Materials and methods

2.1 System modification and probe geometry

A schematic representation of our original benchtop system is shown in Fig. 1. The system consists of a 450 W Xenon Arc lamp (JY Horiba, Edison, NJ) and a scanning monochromator (Gemini 180, JY Horiba) as the source. A fiber optic probe with a core of 19 illumination fibers surrounded by a ring of 18 detection fibers is used for illumination and collection. The individual illumination and collection fibers had a diameter of 200 μm and a numerical aperture (NA) of 0.22. The effective illumination diameter of the probe is 1 mm. The remitted light is collected by the outer ring of detection fibers and coupled through an imaging spectrograph (Triax 320, JY Horiba) and detected by a CCD (Symphony, JY Horiba). The system specifications are described in full detail in previous studies [19, 22].

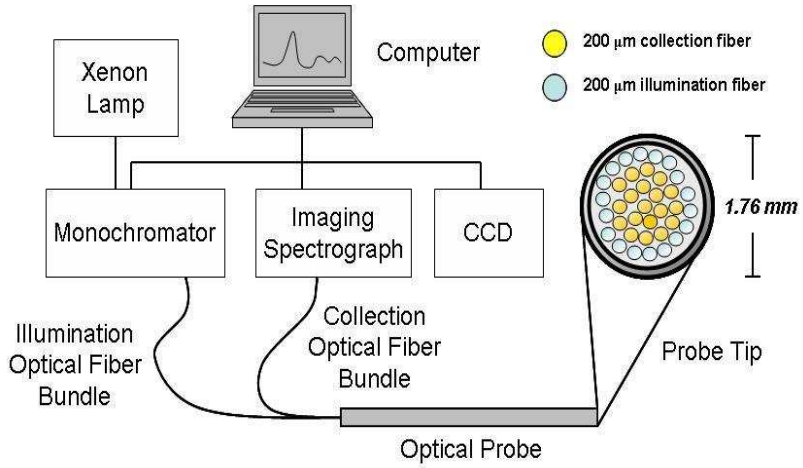

Fig. 1. Schematics of original benchtop system and probe tip.

In this iteration of system modification, the imaging spectrograph and CCD were replaced with a 5.8 x 5.8 mm silicone photodiode (S1227-66BR, Hamamatsu USA). To minimize the separation between illumination and detection areas and to maximize the collection efficiency, a hole with a diameter of 1.3 mm was drilled in the center of the photodiode. The careful drilling of the photodiode minimized mechanical damage and ensured similar detection performance. The only difference between the drilled and un-drilled photodiode was the total

#103335 - $15.00 USD Received 28 Oct 2008; revised 15 Jan 2009; accepted 16 Jan 2009; published 22 Jan 2009

area of detection, which is 32.51 mm^2 for the drilled detector vs. 33.64 mm^2 for the un-drilled detector (the ratio of the areas is 0.97). The ratio of the signals detected by the drilled and un-drilled detectors when exposed to an incandescent bulb was 0.96 which is proportional to the loss in detection area of the un-drilled detector. A single optical fiber with a core diameter of 1 mm and numerical aperture of 0.22 was fitted through the hole to illuminate the sample. Schematics of the system and probe tip are illustrated in Fig. 2. This illumination and collection geometry is similar to that of the fiber optic probe geometry shown in Fig. 1. The photodiode is connected to a photodiode amplifier (PDA-750, Terahertz Technologies Inc., Oriskany, NY) via a coaxial cable for diffuse reflectance measurements. The performance metrics of the original benchtop system and the modified system are also compared.

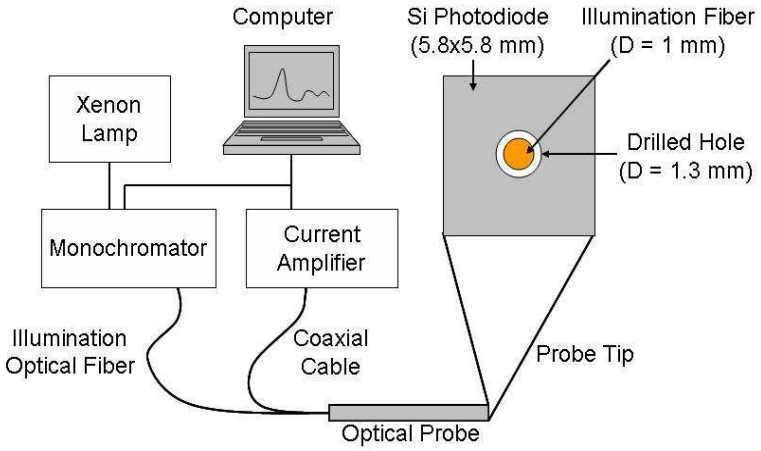

Fig. 2. Schematics of modified diffuse reflectance system and probe tip.

2.2 Optical measurements of synthetic tissue phantoms

To assess the performance of the modified diffuse reflectance spectroscopy system for measuring tissue optical properties, a series of experiments were performed on homogeneous liquid phantoms with absorption and reduced scattering coefficients (μ_a and μ_s') similar to those of human breast tissue in the 400-600 nm wavelength range [23]. Water soluble hemoglobin (H0267, Sigma Co., St. Louis, MO) and 1-μm diameter polystyrene spheres (07310-15, Polysciences, Inc., Warrington, PA) were used as the absorber and scatterer, respectively. The phantoms were made in a 3.5 cm diameter container and filled up to a height of at least 4 cm. A spectrophotometer (Cary 300, Varian, Palo Alto, CA) was used to measure the wavelength-dependent absorption coefficients of the stock hemoglobin solution used to create the phantoms. Prahl's Mie scattering program was used to determine the reduced scattering coefficient [24].

Two sets of liquid phantoms were created and measured. The first set (S1) consisted of seven phantoms of different concentrations (3.7-34.9 μM) of the absorber and a fixed low number for scattering. The second set (S2) consisted of another seven phantoms of the same variable concentrations of Hb as S1, but with a fixed high number for scattering. The low and high scattering phantoms had a wavelength averaged μ_s' of 10-14 cm^{-1} and 16-23 cm^{-1} over 400-600 nm, respectively. A summary of the optical properties of the phantom sets are provided in Table 1.

LabVIEW (National Instruments, Austin, TX) was used to control the monochromator, tuning the light source from 400-600 nm, and to digitally record diffuse reflectance measurements from the current amplifier. Prior to making optical measurements, the slit widths of the monochromator were optimized such that the output power from the illuminating fiber is maximized while the full-width at half-maximum (FWHM) of the lamp

#103335 - $15.00 USD Received 28 Oct 2008; revised 15 Jan 2009; accepted 16 Jan 2009; published 22 Jan 2009

spectrum is 4.5 nm (to resolve the structure of the hemoglobin absorption bands). In the 400-600 nm range, the maximum power was 150 μW at 465 nm, and the minimum power was 50 μW at 600 nm. After a warm up time of 25 minutes, diffuse reflectance spectra were measured over the 400-600 nm wavelength range at increments of 5 nm. The measurements were repeated three times for each phantom to ensure good repeatability. The measurements were made with the room light off and the probe tip in contact with the surface of the liquid phantom. A measurement was also taken from a Spectralon 99% diffuse reflectance standard (SRS-99-010, Labsphere, Inc., North Sutton, NH) with the probe tip in contact with the puck at the end of each phantom study. This spectrum was used to correct for the wavelength-dependent response of the system and throughput of the instrument. For the most absorbing phantom (S2-G) measured in these experiments, the calculated average signal to noise ratio (SNR) over all wavelengths was 60±10 dB, with a minimum SNR of 41 dB at 400 nm and a maximum SNR of 84 dB at 480 nm. SNR_λ is defined as $20*\log (I_{avg,\lambda} / \sigma_\lambda)$, where I is the intensity and σ is the standard deviation at the intensity, obtained from the three repeated measurements.

Table 1. Average optical properties over 400-600 nm for 2 sets of phantoms (μ_a and μ_s' in cm^{-1}, Hb in μM)

Average Optical Properties over 400-600 nm					
	S1		S2		S1 & S2
Phantom	μ_a	μ_s'	μ_a	μ_s'	Hb (μM)
A	0.8	13.6	0.8	23.1	3.7
B	1.7	13.1	1.7	22.2	7.9
C	2.5	12.6	2.5	21.4	11.6
D	3.8	11.9	3.8	20.1	17.5
E	5.0	11.2	5.0	18.9	23.3
F	6.3	10.4	6.3	17.7	29.1
G	7.5	9.7	7.5	16.4	34.9

2.3 Monte Carlo model of reflectance

An inverse Monte Carlo model of reflectance based on a scaling approach was used to extract μ_a and μ_s' of the liquid phantoms. Extensive description of the model theory [16, 17] and optimization of the algorithm for the extraction of biological absorption and scattering properties have been previously reported [22] and is briefly described here.

The diffuse reflectance spectrum is a function of the wavelength dependent absorption and scattering coefficients, determined using the Beer-Lambert law and Mie theory, respectively. In the forward model, the diffuse reflectance spectra for a given range of absorption and scattering coefficients are generated by scaling a single baseline Monte Carlo simulation for a wide range of optical properties, which are then stored in a lookup table. The main assumptions for the model are that the absorbers present in the medium are known and that the scatterers are uniformly distributed single-sized spheres. Hemoglobin is the only absorber, and polystyrene spheres are the only scatterers in this case.

In the inverse model, the measured diffuse reflectance spectrum is fitted to the modeled diffuse reflectance spectrum by iteratively updating the free parameters, which consists of the hemoglobin concentration and the scatterer size and volume density. In our phantom studies, the fixed parameters were the extinction coefficients of the absorber and the wavelength-dependent refractive indices of the scatterer and surrounding medium, which are 1.6 and 1.33, respectively. When the sum of squares error of the modeled and measured spectra is minimized, the optical properties obtained from the extinction coefficients of the absorber and

#103335 - $15.00 USD Received 28 Oct 2008; revised 15 Jan 2009; accepted 16 Jan 2009; published 22 Jan 2009

the wavelength-dependent refractive indices that best predict the measured diffuse reflectance spectrum are extracted.

The probe geometry was modeled by taking a microscopic image of the probe tip and digitally tracing the illumination fiber and the photodiode edges. The image was converted to a binary image that clearly delineates the illumination and detection areas of the probe. Our scalable inverse Monte Carlo model is able to account for very specific probe geometries by convolving the photon collection probability over each source-detector point on the probe.

One of the important parameters of probe geometry that the model takes into account is the NA of the illumination and detection fibers. Since the detection fiber has been replaced by a silicon photodiode, which has no nominal NA, we experimentally obtained the photodiode NA to feed into the MC model as the collection fiber NA. We collimated a laser diode to excite the active area of the photodiode, which is mounted on a rotation stage. With no ambient light in the room, we used the current amplifier to monitor the signal due to the laser while rotating the photodiode to determine the maximum acceptance angle. A measured acceptance angle of 75° in air gave us an NA of 0.965 for the photodiode.

To calibrate for system throughput and wavelength dependence, the experimentally measured and modeled spectra of the target phantom were normalized to that of a reference phantom with predefined optical properties at each wavelength. Phantom B in phantom set 2 (a low-absorbing phantom with μ_a = 1.7 cm^{-1} and μ_s' = 22.2 cm^{-1}) was used as the reference phantom to calibrate every other phantom as targets within each phantom set. The reference phantoms were chosen based on the suggestion proposed by a comprehensive study on the robustness of the inverse MC model in extracting a wide range of optical properties [22]. Bender *et al*. suggested using reference phantoms with mid to high reduced scattering coefficients (μ_s' = 15-25 cm^{-1} over 400-600 nm) and low to mid absorption coefficients (μ_a = 0.5-2.5 cm^{-1} over 400-600 nm). Optical properties at each wavelength were extracted for each target phantom, and the inversion errors were averaged over all wavelengths and phantoms. The inversion errors were evaluated based on the following criteria. Extracted errors of less than 10% are considered excellent while errors of 10~20% are fair. Errors above 20% in phantoms are considered high and may or may not accurately extract physiological parameters in tissue.

2.4 Simulation of wavelength reduction

To further decrease the cost and size of our benchtop system in the future, we investigated the potential of replacing the Xenon lamp and monochromator by using several inexpensive LEDs in the 400-600 nm range. This feasibility study consisted of performing simulations of wavelength reduction on the measured liquid phantom data obtained with our modified system. 5 commercially available LED wavelengths in the 400-600 nm spectral range were chosen: 405, 450, 470, 530, and 590 nm.

The key assumption in the simulation was that each wavelength has a bandwidth of 20 nm with a Gaussian distribution. This was an approximation made based on the commercially available LED specifications. The collected spectra from the phantom studies were processed such that data points from all wavelengths were excluded, except for those of the LED wavelengths enumerated previously. Each originally measured phantom spectrum, which consisted of 41 wavelengths over the 400-600 nm range in 5 nm increments, was first convolved with each of the 5 Gaussian-distributed LED emission spectra separately. This generated 5 individual new spectra. Then the new spectra were integrated over 100 nm, an arbitrarily large value that spans much wider than the LED bandwidth of 20 nm, to account for all potential signals from the LEDs. The integration was necessary because with a single photodiode, one can only measure the integrated intensity of the new spectrum. The resulting 5 intensities are the signals that would be measured using those specific LEDs. The final wavelength-reduced spectrum for each of the phantoms was composed of only these 5 data points. These newly generated LED spectra were used to extract optical properties.

#103335 - $15.00 USD Received 28 Oct 2008; revised 15 Jan 2009; accepted 16 Jan 2009; published 22 Jan 2009

2.5 Simulation of crosstalk analysis

A primary goal in the future iterations of device design involves multiplexing the single-pixel device presented in this article into a quantitative spectral imaging device. This can be done by arranging multiple optical fiber-photodiode pairs in a matrix formation. An important new parameter that must be characterized is the crosstalk. In an ideal situation, a fiber-photodiode pair is to be treated as a single pixel; however, the issue of a detector collecting stray light from an adjacent pixel, or even from multiple adjacent pixels, is unavoidable. High levels of crosstalk can significantly affect the measurement accuracy from tissue directly below the pixel.

To demonstrate feasibility of implementing a quantitative spectral imaging device, a Monte Carlo forward model of reflectance as described in the previous section was used to simulate a design where the nine Hamamatsu S1227-66BR photodiodes, each with 1.3 mm holes drilled in the center, were packed as closely together in a 3x3 matrix as shown in Fig. 3. Each fiber is 1 mm in diameter and has an NA of 0.22. The silicon photodiode NA is 0.965. The separation of adjacent fibers is 8.48 mm. A forward model based on this geometry was used to generate the diffuse reflectance spectrum including both signal and cross-talk for each pixel. The simulated spectrum from each pixel was then inverted independently to determine the effect of cross-talk on the extracted optical properties.

The extracted errors due to the presence cross-talk were estimated by simulating phantom measurements with hemoglobin as the absorber and polystyrene spheres as the scatterer. Measurements were simulated for five phantoms with a wide range of average absorption coefficients over 400-600 nm (μ_a = 0.4, 0.9, 1.3, 1.6, 2.0 cm^{-1}) and a fixed reduced scattering coefficient (μ_s' = 10). The inversion accuracy in the presence of crosstalk not only provides feasibility of creating such a device, but also useful information for future design parameters, such as fiber size, detector size, and pixel spacing.

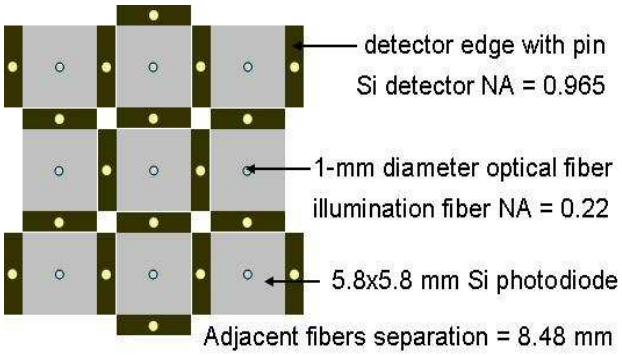

Fig. 3. A 3x3 imaging array used for simulating crosstalk

3. Results and discussion

3.1 Comparison of original benchtop system with modified system

The purpose of our study was to modify our benchtop system to decrease its size and cost of while still achieving comparable performance in extracting tissue optical properties. The modification of the benchtop system not only impacts size and cost but also the ability to seamlessly multiplex the device into a quantitative spectral imaging system. Comparisons of the throughput-related parameters and system characteristics of the original and modified systems are presented in Table 2.

Because the benchtop system is capable of also acquiring fluorescence information while the modified system can only be used for reflectance in its current form, we recognize the inherent limitations of the side-by-side comparisons of various parameters of the benchtop

#103335 - $15.00 USD Received 28 Oct 2008; revised 15 Jan 2009; accepted 16 Jan 2009; published 22 Jan 2009

and the modified system. In its current form, the modified system uses a monochromator to tune the light from the Xenon lamp from 400-600 nm, which is directly illuminated onto the sample. On the other hand, the original system uses only white light to illuminate the sample, and the collected light is then split by the spectrograph. The monochromator was used in this particular instance because it was readily available. Because the monochromator is relatively slow in scanning a range of wavelengths, taking over a minute for a measurement, a filter wheel can be implemented in the place of the monochromator to speed up data acquisition if the next iteration of system design requires a tunable source.

Table 2. Comparison of throughput-related parameters of original and modified systems

	Original System	**Modified System**
Illumination Sources	Xenon lamp and Monochromator (Reflectance and Fluorescence)	Xenon lamp and Monochromator (Reflectance only)
Effective Illumination Diameter	1.00 mm	1.04 mm
Illumination NA	0.22	0.22
Detection Areas	2.26 mm^2	32.31 mm^2
Detection NA	0.22	0.96
Sensing depth (over 400-600 nm)	0.6 – 1.4 mm (μ_a = 0.5~2.5 cm^{-1}, μ_s' = 10~20 cm^{-1})	0.4 – 1.7 mm (μ_a = 0.5~2.5 cm^{-1}, μ_s' = 10~20 cm^{-1})
Detector QE	35% (400~600 nm) Min: 26% @ 450 nm Max: 45% @ 600 nm	73% (400~600 nm) Min: 62% @ 400 nm Max: 79% @ 600 nm
Dark Noise	6.4 x 10^{-7} pA	20 pA
Readout Noise	4.2 x 10^{-9} A	1 x 10^{-12} A
SNR (400~600 nm) (μ_a=7.5 cm^{-1}, μ_s'=16 cm^{-1})	Average: 45 ± 5 dB Min: 32 dB @ 405 nm Max: 60 dB @ 550 nm	Average: 60 ± 10 dB Min: 41 dB @ 400 nm Max: 84 dB @ 480 nm
Cost of Detection System	> $20,000	$1,000

Since the effective illumination diameter and source detector separation are similar for both systems, the sensing depth is also similar over the same range of wavelengths for a given set of optical properties. Monte Carlo simulations were performed to assess sensing depth for

#103335 - $15.00 USD Received 28 Oct 2008; revised 15 Jan 2009; accepted 16 Jan 2009; published 22 Jan 2009

both probes over 400-600 nm for the optical properties, μ_a = 0.5-2.5 cm^{-1} and μ_s' = 10-20 cm^{-1}. The sensing depth is defined as the depth at which 90% of the probable visited photons in the sample will exit and reach the detector to be collected. The modified system has a slightly deeper sensing depth because the detection area is bigger and can collect photons that have traveled deeper into the medium although these exit photons farther away from the illumination fiber have much less weight than those that are closer to the illumination fiber. The sensing depth can be easily changed by adjusting various source-detector separations and is an important parameter to consider in future probe designs, depending on the clinical application for which the technology will be used.

While some parameters, such as sensing depth and effective illumination area, are comparable for both systems, the modified system has several parameters that are superior to those of the original system, which ultimately translate to high signal-to-noise (SNR), and lower cost. Based on the commercial specification sheets, the CCD of the benchtop system has an average quantum efficiency of 35% from 400-600 nm. On the other hand, the photodiode in the modified system has an average quantum efficiency of 73% in the same range. Furthermore, the detector is directly in contact with the sample in the modified design, collecting most of the remitted light, whereas the detector of the benchtop system is at the distal end of the collection fiber bundle where significant light is inherently lost. The average SNR in a dark, highly absorbing phantom (μ_a = 7.5 cm^{-1} and μ_s' = 16 cm^{-1}) measured using benchtop system is 45±5 dB over 400-600 nm, which is lower than the 60±10 dB measured with the modified system. In addition, the cost of the detection portion of the modified system is significantly cheaper compared to its benchtop counterpart.

3.2 Synthetic tissue phantom studies

Monte Carlo inversions were performed to extract optical properties on both sets of phantoms. Figure 4 shows the extraction performance using the modified system along side the original benchtop system. For the modified system, the correlation coefficients for expected and extracted μ_a and μ_s' are 0.9992 and 0.9478, respectively. Using phantom S2-B (μ_a = 1.7 cm^{-1} and μ_s' = 22.2 cm^{-1}) as the reference, the overall extracted μ_a error was 9.8±5.0%, and the overall μ_s' error was 7.6±4.2%. For this similarly wide range of optical properties and using a similar reference phantom (μ_a=1.4 cm^{-1}, μ_s'=19.3 cm^{-1}), the original benchtop system had overall errors of 9.8±8.2% and 7.7±6.3% for μ_a and μ_s', respectively. All percent error values given are mean RMS percent errors averaged across all wavelengths for all target phantoms for the extraction of optical properties. The modified system and the original benchtop system seem to have very comparable performance in extracting optical properties in tissue phantoms over a wide range of optical properties.

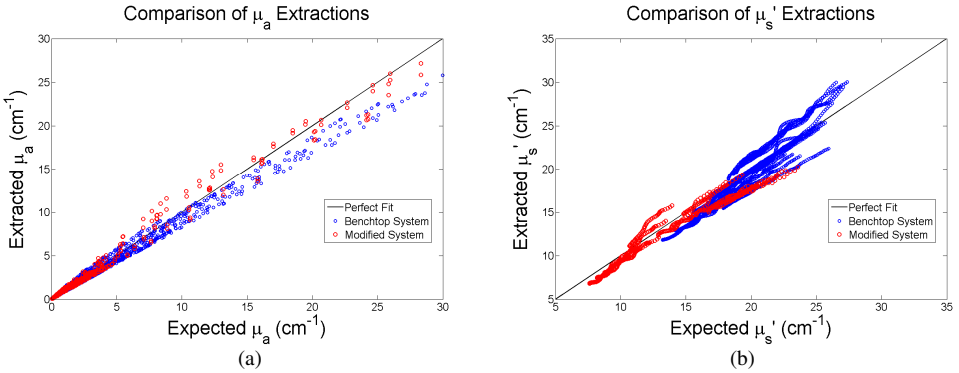

Fig. 4. Comparison of (a) μ_a and (b) μ_s' extractions by the original benchtop and modified systems.

#103335 - $15.00 USD Received 28 Oct 2008; revised 15 Jan 2009; accepted 16 Jan 2009; published 22 Jan 2009

3.3 Simulated wavelength reduction

Figure 5 shows the measured reflectance spectra of the lowest and highest absorbing phantoms for all wavelengths and the generated data points from the wavelength reduction simulation used for additional MC inversions, both calibrated by the puck spectrum. It is important to note that the simulated wavelength-reduced spectra are composed on only 5 data points each. These 5 data points are the signal that would be read by the photodiode current amplifier.

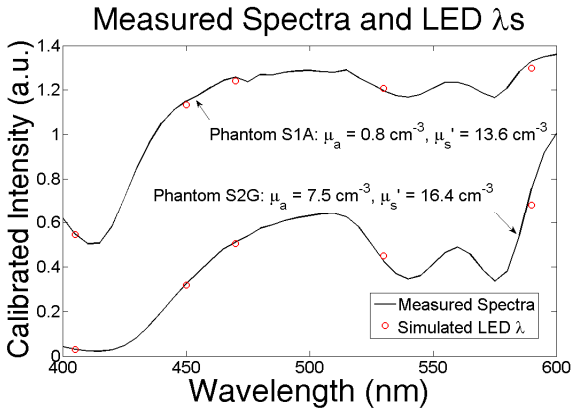

Fig. 5. Experimental reflectance spectra from lightest and darkest phantoms with the 5 wavelengths chosen to for MC inversions

Figure 6 illustrates the theoretical extraction performance of the modified system after wavelength reduction simulations. For the same large range of optical properties and using the same reference phantom as before (S1-B: μ_a = 1.7 cm^{-1} and μ_s' = 22.2 cm^{-1}), the overall μ_a extraction error was 9.6±5.8%, and the overall μ_s' error was 14.3±7.3%. The correlation coefficients for expected and extracted μ_a and μ_s' are 0.9972 and 0.8628, respectively, in the inversion of wavelength-reduced phantom data. The increase in the extraction errors can be attributed to not only the reduction of wavelengths, but also the loss of spectral information with a wider FWHM (20 nm) of the simulated wavelength reduction.

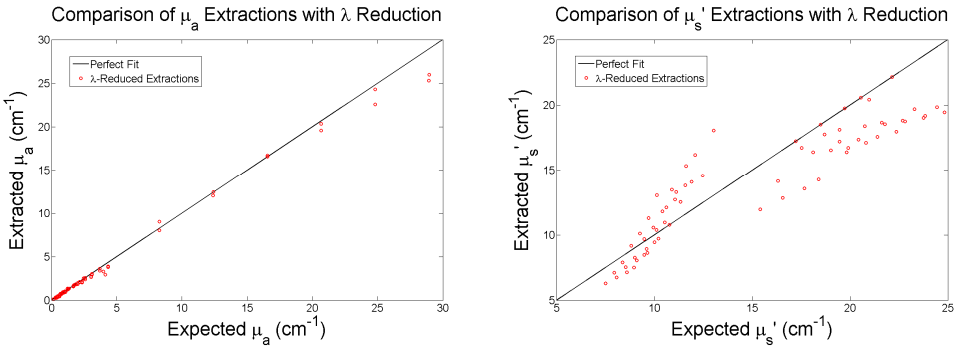

Fig. 6. Extractions of (a) μ_a and (b) μ_s' after wavelength reduction simulation

Using only 5 wavelengths from the collected phantom data to perform the Monte Carlo inversion, the hemoglobin spectra can be reconstructed with the extracted absorption coefficients and the molar extinction coefficient for hemoglobin measured with the spectrophotometer on the day of the phantom study. Figure 7(a) shows the reconstructed

#103335 - $15.00 USD Received 28 Oct 2008; revised 15 Jan 2009; accepted 16 Jan 2009; published 22 Jan 2009

hemoglobin spectra averaged over all phantoms. Figure 7(b) shows relatively good extraction accuracy for hemoglobin concentrations for all phantoms. There is a slight underestimation of hemoglobin at very high concentrations, which is consistent with previous studies using the benchtop system [22].

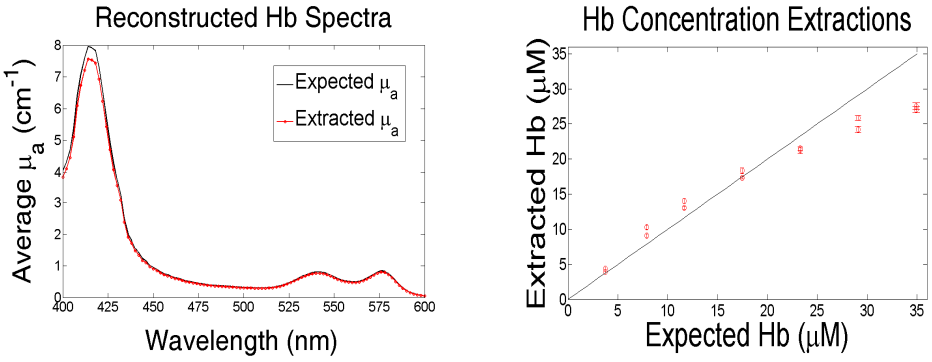

(a) (b)

Fig. 7. (a) Reconstructed Hb spectra averaged over all phantoms using extracted μ_a values at the 5 chosen wavelengths; (b) Extractions of Hb concentration by inverting wavelength-reduced data

These wavelength reduction results show the feasibility of replacing the Xenon Arc lamp and the monochromator in our modified system with just 5 LEDs in the next generation of system design. Not only is there an abundance of high-powered LEDs in the 400-600 nm range, these potential light sources are also very inexpensive. Furthermore, the use of LEDs can potentially obviate the need for optical fibers and is well-suited for miniaturized optical spectral imaging systems. With LEDs as the illumination source and tiny photodiodes as the detector, the device would then be truly miniaturized compared to the current benchtop system while still achieving comparable performance in the extraction of optical properties in tissue. It is reasonable to believe that an LED-photodiode device would have not only the benefits of having the superior collection efficiency of the detector, but also higher throughput with high-powered LEDs. In addition to LEDs as an alternative source, a combination of a lamp and a series of band-pass filters may also be implemented. The use of band-pass filters in conjunction with an optical fiber can also provide high throughput similar to LEDs and is relatively simple to integrate into the existing benchtop system. However, the down side of using the latter approach is the increased cost and size of a lamp-filter wheel based system. The enumerated errors of the extraction of optical properties shown in Table 3 indicate that it is unnecessary to use the full 400-600 spectrum to extract optical properties with good accuracy.

Table 3. A table of comparison for the original benchtop system and modified system with its wavelength-reduced inversion errors, averaged for all reference-target phantom combinations

Summary of Optical Properties and Inversion Errors					
(400-600 nm)	Avg μ_a range	Avg μ_s' range	Hb range	μ_a error	μ_s' error
Original System	0.2~8.2 cm^{-1}	16.9~24.1 cm^{-1}	1.0~35.2 μM	9.8±8.2%	7.7±6.3%
Modified System	0.8~7.5 cm^{-1}	9.7~23.1 cm^{-1}	3.7~34.9 μM	9.8±5.0%	7.6±4.2%
λ-Reduced	0.8~7.5 cm^{-1}	9.7~23.1 cm^{-1}	3.7~34.9 μM	9.6±5.8%	14.3±7.3%

#103335 - $15.00 USD Received 28 Oct 2008; revised 15 Jan 2009; accepted 16 Jan 2009; published 22 Jan 2009

We recognize the importance of wavelength choice when the system is to be used in clinical situations in the future. The phantoms presented in this study are very simplified compared to the composition of real human tissue. However, we know from numerous studies that hemoglobin is the dominant absorber in tissue. We can extract its concentration with good accuracy with a few wavelengths. The current wavelength choices presented in this study sufficiently encompass the distinct features of hemoglobin: the Soret, α-, and β-bands. Oxy- and deoxy-hemoglobin and thus hemoglobin saturation can be extracted because of the clear shifts in spectral peaks. These are important parameters to delineate normal from malignant tissues, which is an important goal. Other physiological parameters may also be quantified using just a few wavelengths, analogous to other systems currently in clinical studies, such as those using frequency domain photon-migration techniques [25]. If more than 5 wavelengths are needed to accurately extract other important physiological parameters, a system with a lamp and filter wheel can be designed to accommodate as many as 10 wavelengths. The addition of a few extra LEDs can also be implemented.

3.4 Simulated crosstalk analysis

Crosstalk was simulated as a preliminary effort to create an imaging device. We hypothesized that the center pixel in the 3x3 matrix, shown previously in Fig. 3, would receive the most amount of crosstalk and thus is presented as the worst case scenario. As expected, the inversion showed that center detector had the worst extraction errors for μ_a and μ_s'. Table 4 enumerates the inversion errors in the presence of crosstalk at the center, the side, and the corner detectors, respectively.

Table 4. μ_a and μ_s' extraction errors (%) for each detector in the presence of crosstalk in phantoms ranging from low to high absorption coefficients (μ_a = 0.4 - 2.0 cm^{-1}) and mid reduced scattering coefficients (μ_s' = 10 cm^{-1}), averaged for all reference-target phantom combinations.

Inversion errors with crosstalk						
	Center Detector		Side Detectors		Corner Detectors	
Phantoms	μ_a error	μ_s' error	μ_a error	μ_s' error	μ_a error	μ_s' error
A	2.2	7.8	1.6	5.7	1.0	2.9
B	2.2	5.1	1.6	3.6	0.9	1.8
C	2.4	5.0	1.6	3.3	0.9	1.8
D	3.6	6.5	1.8	3.8	1.3	2.3
E	4.3	8.1	2.4	4.8	1.7	3.1

The errors were averaged over all reference-target phantom combinations. With μ_a and μ_s' extraction errors of less than 2% and 5%, respectively, the simulation shows that crosstalk has little effect on the side and corner detectors. The center detector received the most crosstalk, and its extraction errors are nearly doubled compared to those of the non-center detectors. Simulation shows that the overall errors due to crosstalk are relatively small and that constructing an imaging device will be feasible based on this particular geometry. Other factors that could reduce crosstalk errors in the multi-pixel device prototype are fiber size, detector size, and detector spacing. It is important to note that crosstalk was only generated to evaluate its effect on inversion errors in this study. It should also be noted that crosstalk was not taken into account by our current Monte Carlo model. Work is currently being done on creating a fast multi-region Monte Carlo model that is capable of including the effects of cross-talk.

The 3x3 matrix simulated in this study was strategically created partially based on the probability of exiting photons hitting adjacent detectors being very small. The drawback of this design is that the detectors themselves as well as the pixel spacing have to be large. While

#103335 - $15.00 USD Received 28 Oct 2008; revised 15 Jan 2009; accepted 16 Jan 2009; published 22 Jan 2009

such a device is able to show a proof of concept in creating an imaging device, it may not be useful clinically to have a matrix of large detectors spaced far apart from each other. Once crosstalk is modeled effectively, the imaging prototype can be designed with smaller detectors and pixel spacing with better resolution for clinical applications.

4. Conclusions

This multi-faceted study shows that the modified system along with our Monte Carlo model can be miniaturized and extended into an optical spectral imaging system. In its current, single-pixel state, the system is capable of extracting optical properties in tissue phantoms with good accuracy in the 400-600 nm range comparable to the clinical benchtop system. By placing the detector directly in contact with the sample, the collection efficiency is improved. Furthermore, the results from the wavelength reduction simulations from the measured phantom data show great potential in replacing the lamp and monochromator with several high powered LEDs in the 400-600 nm range for higher throughput, smaller size, and much lower cost. By strategically choosing high powered LEDs with a 20-30 nm bandwidth while covering most of the 400-600 nm range, an LED-photodiode device can be created and used to extract a similar range of tissue optical properties within a well-defined sensing depth. The new semiconductor device would not only undoubtedly have higher throughput than the lamp-monochromator model, but also be truly miniaturized and made at a fraction of the cost of the original system. Lastly, the crosstalk analysis shows the potential for either the fiber-photodiode system or the miniaturized LED-photodiode system to be multiplexed into an imaging device. With a low probability of exiting photons reaching adjacent detectors, the effect of crosstalk on inversion accuracy is low for a matrix of 5.8x5.8 mm silicon photodiodes. By accurately accounting for crosstalk with our Monte Carlo model, an imaging prototype can be made with much smaller detectors spaced closer to one another. The use of smaller, more sensitive detectors along with sources with superior throughput would ultimately result in a system with high clinical utility.

The eventual goal of creating a miniaturized spectral imaging device based on inexpensive photodiodes and LEDs can have a remarkable impact in not only basic biomedical research, but also in clinical situations worldwide. While a single-pixel probe is certainly useful for small regions of tissue, the information that can be unraveled by an imaging device is unmatched for larger samples, such as those in tumor margin assessment, assessing tumor response to therapy, epithelial pre-cancer and cancer detection, among other applications. A miniaturized imaging device based on the LED-photodiode design would be able to spectrally map out quantitative biological information for tissue composition just below the surface. Furthermore, the device would be portable and inexpensive, useful and accessible for not only the standard research laboratory or clinic, but also for rural clinics in the developing world.

Acknowledgments

This project was supported by the Era of Hope Scholar Award from the Department of Defense Breast Cancer Research Program awarded to Dr. Nirmala Ramanujam.

#103335 - $15.00 USD Received 28 Oct 2008; revised 15 Jan 2009; accepted 16 Jan 2009; published 22 Jan 2009